Prepared for submission to JINST

ARDESIA-16: a 16-channel SDD-Based Spectrometer for Energy Dispersive X-ray Fluorescence Spectroscopy

G. Utica,[a,b,1] **E. Fabbrica,**[a,b] **M. Carminati,**[a,b] **G. Borghi,**[c,d] **N. Zorzi,**[c,d] **F. Ficorella,**[c,d] **A. Picciotto,**[c,d] **I. Allegretta,**[e] **G. Falkenberg**[f] **and C. Fiorini**[a,b]

[a] *Politecnico di Milano - Dipartimento di Elettronica, Informazione e Bioingegneria DEIB, Via Giuseppe Ponzio, 34/5, 20133 Milano MI, Italy*

[b] *Istituto Nazionale di Fisica Nucleare INFN - Sezione di Milano, Via Giovanni Celoria, 16, 20133 Milano MI, Italy*

[c] *Trento Institute for Fundamental Physics Applications TIFPA, Via Sommarive, 14, 38123 Povo TN, Italy*

[d] *Fondazione Bruno Kessler FBK, Via Sommarive, 18, 38123 Povo TN, Italy*

[e] *Università degli Studi di Bari, Dipartimento di Scienze del Suolo, della Pianta e degli Alimenti (Di.S.S.P.A.), Via Giovanni Amendola, 165/a, 70126 Bari BA, Italy*

[f] *Deutsches Elektronen-Synchrotron DESY, Notkestraße 85 22607 Hamburg, Germany*

E-mail: gianlorenzo.utica@polimi.it

Abstract: We present ARDESIA-16, an X-ray spectrometer based on a monolithic 16-element Silicon Drift Detector (SDD) matrix specifically designed for synchrotron applications. In this work, we describe the main design guidelines which we followed concerning the signal throughput, the energy efficiency, the energy resolution and the overall solid angle covered by detector elements. The characterization of the spectrometer has been made both with radioactive sources in a laboratory environment and with synchrotron light at the P06 beamline (DESY, Hamburg). Experimental results showed an average energy resolution at the optimum peaking time equal to 125 eV (FWHM at Mn Kα), a maximum achieved Output Count Rate (OCR) equal to 17 Mcps, an increase of the energy efficiency above 10 keV thanks to the 1mm-thick SDD and an overall solid angle equal to 0.4 sr. Finally, we report the first X-ray fluorescence microscopy (XFM) images acquired with an ARDESIA spectrometer.

Keywords: X-ray detectors; Instrumentation for synchrotron radiation accelerators; X-ray fluorescence (XRF) systems; Solid state detectors

[1]Corresponding author

Contents

1 Introduction

In the last few years, new generations of synchrotron light sources and new cutting-edge beamlines pushed the development of more performing energy dispersive X-ray fluorescence spectrometers. To cope with extremely brilliant X-ray beams, fluorescence detectors must overcome their nowadays maximum throughput keeping ultralow noise performance to attain the required high energy resolution. This work has been carried out within the framework of the ARDESIA (ARray of DEtectors for Spectroscopy and Imaging Applications) project [1–3]. The goal of this project is to develop a spectrometer based on multielement monolithic Silicon Drift Detector (SDD) matrices with high count rate capability for applications like fluorescence mode X-ray absorption spectroscopy (XAS) [4, 5], X-ray fluorescence (XRF) spectroscopy and X-ray fluorescence microscopy (XFM) imaging [6, 7] which are widespread across a range of fields (e.g. medicine, biology, geology, chemistry, physics). Those applications are often very time-consuming and beamline users demand longer acquisition time to improve counting statistics in elemental imaging. For this reason, beamline scientists foster the development of high count rate spectrometers to optimize beam time assigned to experiments.

A typical approach to develop an X-ray fluorescence spectrometer is to use solid state detectors, as for example in refs. [8–12]. To minimize the intrinsic noise introduced by detectors, large area detection system are mainly based on SDD instead of PIN diode, allowing a reduction of the input capacitance which becomes independent from the detector active area [13, 14]. Another approach to achieve high energy resolution is to use Transition Edge Sensor (TES) [15, 16], energy resolution is currently ten times better than SDDs which are limited by the statistical fluctuation of the generated charge [17] in the active volume. However, this technology is still limited in count rate capabilities (i.e., few counts per second per pixel).

The design of a low-noise front-end electronics to read SDD signals is crucial with short processing

time, required for fast photon detection. A decade ago, a ultralow-noise CMOS charge preamplifier, named "CUBE" [18–20], was proposed as an alternative SDD readout solution with respect to the more commonly used solution implementing an integrated JFET on the detector substrate [21, 22]. Such approach became rapidly the state-of-the-art front-end ASIC to readout SDD in commercial systems. Other low-noise CMOS readout solutions for SDDs have also been published in [23, 24]. In synchrotron beamlines, the analog outputs of a charge preamplifier are typically read out by Digital Pulse Processors (DPP) which allow the spectrometer to reach a higher count rate with the respect to Analog Pulse Processors (APP). However, APPs show lower cost per channel and higher integration capability making them suitable for detector system with large number of channels. A detailed comparison of DPP with APP can be found in Hafizh et al. [25].
A key figure-of-merit for fluorescence detection system is the maximum Output Count Rate (OCR) that assesses the maximum photon rate correctly processed by the system. The OCR of each detector element is limited by the readout electronics (i.e., both front-end and back-end) and the collection time of the charge at the anode of the detector. Remarkable results have been obtained employing single element SDD coupled with CUBE preamplifier and Falcon-X (XIA, California, USA) Digital Pulse Processors leading to an OCR > 3 Mcps [26]. Another straightforward way to further improve the overall OCR of a spectrometer is to increase the number of SDD elements and consequently the number of electronics channels. Usually, the approach followed for the development of multichannel fluorescence spectrometers is to arrange single elements next to each other. This would lead to a large dead area among elements and a not optimized solid angle because of the termination structure surrounding the detector active area and mechanical constraints of single detection unit used in the assembly.

The strategy we followed in ARDESIA development is to use a multichannel monolithic SDD array coupled with custom design 4-channel CUBE preamplifiers. The project started in 2016 in collaboration with Istituto Nazionale di Fisica Nucleare (INFN) and Politecnico di Milano. We developed two first prototypes based on 4-element SDD monolithic matrices [1–3]. The two prototypes have been installed in two different beamlines: one at the LNF (Frascati, Italy) DAΦNE-Light DXR1 soft X-ray beamline and one at the LISA CRG beamline at the ESRF (Grenoble, France). After achieving satisfactory results with these two prototypes, we started to develop a new spectrometer with higher number of channels and thicker substrate to gain in count rate capability and quantum efficiency at higher energy range. In this work, we report the design and the characterization of the 16-element detection module and the ARDESIA-16 spectrometer. Finally, we show the results of the first synchrotron qualification of the spectrometer at P06 beamline (DESY, Hamburg) [27, 28].

2 Detection Module

2.1 Structure

Typical SDD structure is reported in figure 1. The fabrication process is a double-side technological process made on a high-resistivity floating-zone silicon wafer. The device has an asymmetric structure with the collecting electrode (i.e., anode), the drift junction electrodes (i.e., rings) and the voltage divider on one side (i.e., front side) and the radiation entrance window on the other side

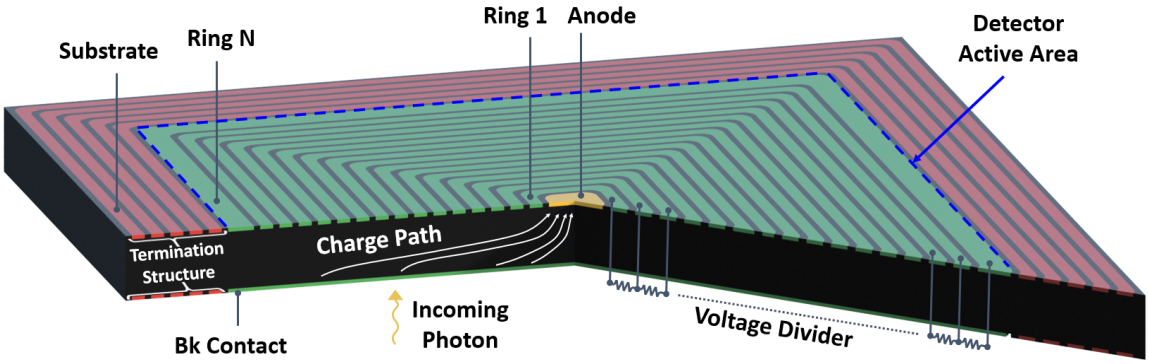

Figure 1: Simplified working principle of a single-element SDD (not to scale).

(i.e., back side). The entrance window is realized with a uniform junction defining the device active area. The integrated voltage divider on the front side feeds the voltages to all the rings by applying only two voltages on ring 1 and ring N. Therefore, the biasing is achieved by means of five contacts: ring 1, ring N, anode, back and substrate. Thanks to its peculiar structure, SDD allows to collect the signal charge through a small anode ($< 100\ \mu m \times 100\ \mu m$) independent from the detector active area.

The novel detection module is based on a 16-channel monolithic SDD matrix (figure 2a) produced at Fondazione Bruno Kessler (Trento, Italy). The single pixel features a square geometry, 5 mm side, and the total die area is 24 mm × 24 mm. An emerging trend is to produce SDD with thicker substrate to extend the energy range in which the detector is efficient. In the first production at FBK, SDDs were 450 μm thick. In the second production, we have also developed and produced thicker SDDs (800 μm and 1000 μm thick) to enhance quantum efficiency for higher energy range (i.e., $> 10\ keV$). For thicker SDDs, a higher operating bias was expected due to the increased depletion voltage. To reduce this effect, thick devices were realized using silicon substrates with a

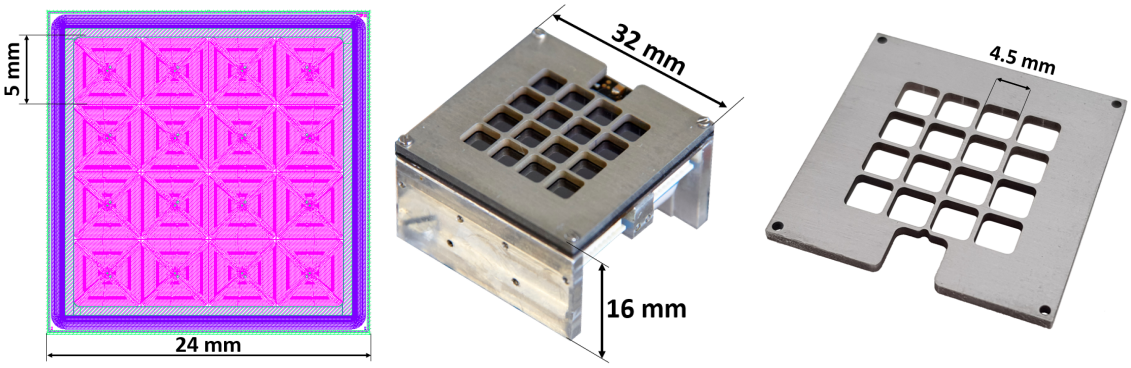

(a) (b) (c)

Figure 2: ARDESIA-16 detection module. (a) The detector is a 4 × 4 array of square SDDs, each element area is equal to 5 mm × 5 mm. (b) The assembled detection module is reported as well as the molybdenum mask (c).

higher resistivity. Even so, the extension of the depleted regions would increase, therefore a partial re-design of the SDD was required. In facts, 1) the drift ring geometry was changed to avoid a drop of linearity in the voltage divider due to punch-through effects; 2) the termination structure was enlarged so that it could handle a higher voltage drop avoiding risk of breakdown; 3) the border electrodes (i.e., ring and back contact) were enlarged to avoid a reduction of the effective active area.

In figure 2b, the detection module is reported. The detector array is glued to a Printed Circuit Board (PCB) and anchored to an aluminum block along with a Molybdenum collimator to mask the regions at the pixel borders in order to prevent charge sharing between adjacent SDD elements. Each hole of the mask is 4.5 mm × 4.5 mm (figure 2c), leading to a collimated area equal to 20.25 mm^2 per SDD element. The aforementioned PCB hosts bypass capacitors and 16 CUBE preamplifiers (i.e., four monolithic 4-channel CUBE ASICs) whose inputs are wedge-bonded to SDD anodes to perform the signal readout. Gluing the front-end electronics and the detector on the two faces of only one PCB substrate resulted in a small size package with a total volume of the detection module equal to 32 mm × 32 mm × 16 mm. Aiming at preventing further size increase, the connection to the back-end electronics is carried out from the bottom of the detection module through 4 Flat Flexible Cables plugged in 4 vertical connectors.

2.2 Characterization Setup

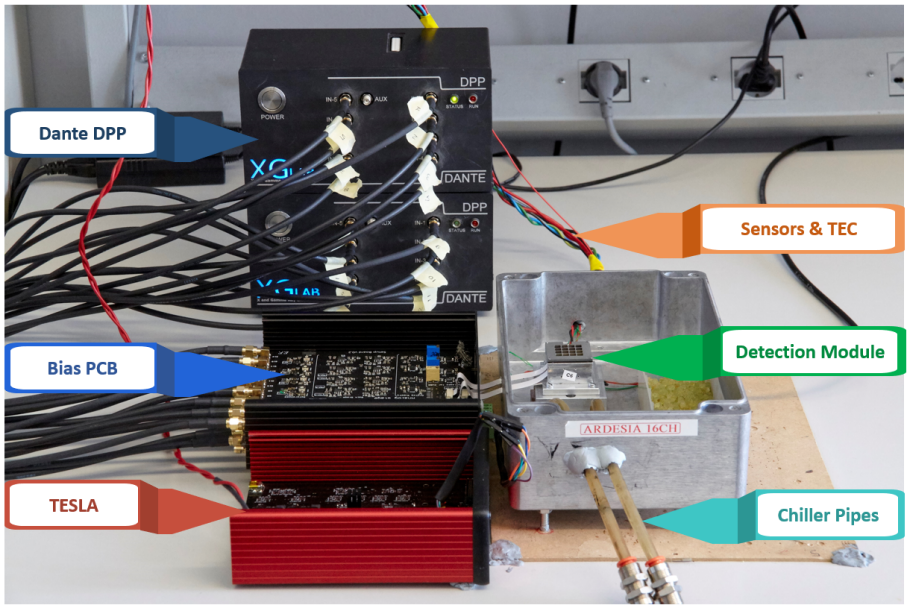

Figure 3: Characterization setup of the detection modules.

Once the detection module was assembled, we characterized it by means of spectroscopy measurements in a dedicated setup (figure 3). The detector was placed in a light-tight aluminum box. The relative humidity inside the box was kept below 5% both by fluxing nitrogen and placing silica gel beads. The detection module was cooled down with a thermoelectric cooler (TEC) module whose hot face is kept at a controlled temperature by means of a water cooled heatsink and

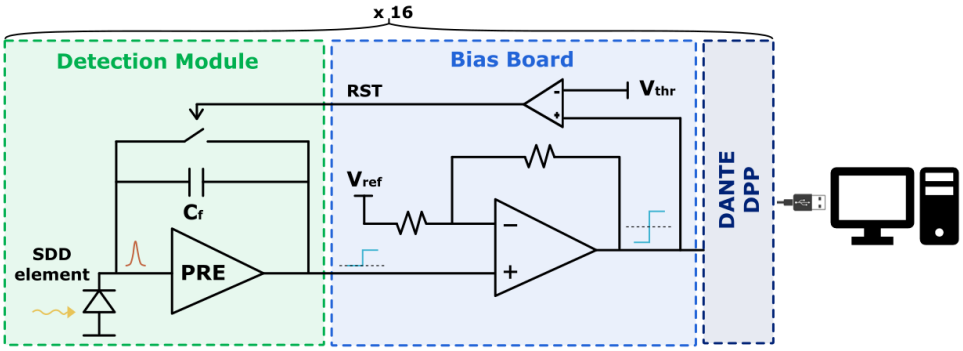

Figure 4: Schematic view of the electronics channel from SDD element to DPP.

a chiller. A custom-design power supply unit (Tesla [2]) feeds the supply to the Bias PCB. The Bias PCB performs three tasks: 1) manages the signal conditioning of the preamplifier outputs so that compatibility to the DPP dynamic range is achieved, 2) delivers a programmable threshold-sensitive reset to all preamplifiers, which is synchronous to all channels, and 3) feeds ultralow noise reference and supply voltages to the 16 preamplifiers and to the SDD matrix. The schematic view of the signal path along an electronics channel is depicted in figure 4. The photo-generated charge is integrated by the preamplifier and converted into a voltage signal. A selectable-offset and fixed-gain analog stage matches the signal voltage swing with the dynamic range of the DPP. Finally, the channel outputs of the Bias PCB are connected to the DPP through 16 coaxial cables. The DPPs used for the characterization are two 8-channel DANTE DPP (XGLab, Italy) connected in daisy-chain configuration. This DPP provides a versatile solution for characterizing the detector and achieving high count rates using conventional (i.e. trapezoidal) filtering. It is known that ultrahigh counting rates performances may be achieved in experiments using high-end DPPs [29].

2.3 Experimental Results

We assembled and characterized 7 monolithic detection modules: three 450 μm thick array and two for each of the two other thicknesses. They showed an overall channel yield higher than 96% (i.e., number of working channels over the total number of tested channels). In figure 5a, we report a measurement of one detection module based on a 450 μm thick array and with all working channels. ^{55}Fe was used as an X-ray source whose decay process produces Mn K fluorescence X-rays. The detector has been cooled down to -30 °C. We evaluated the energy resolution as the Full Width at Half Maximum (FWHM) of Mn Kα resulting in the range of 123.3 ÷ 127.2 eV for all channels with an average value equal to 125 eV. The DPP applies a trapezoidal filtering whose peaking time for those spectra was set to 3 μs and the flattop was set to 128 ns. The energy resolution of each channel of a 450 μm thick detector is reported in figure 5b together with the results of a 1000 μm thick detection module. Despite the higher quantum efficiency at high energy, the latter shows lower energy resolution performances because of the higher leakage current and the longer collection time of the charge. Outcomes of the 800 μm thick detector are comparable with the 1000 μm thick and, thus, they are not reported in this paper.

A key parameter assessing the quality of the device entrance window is the peak-to background (PTB). PTB is defined as the maximum amplitude of the Mn Kα line from a ^{55}Fe radioactive source

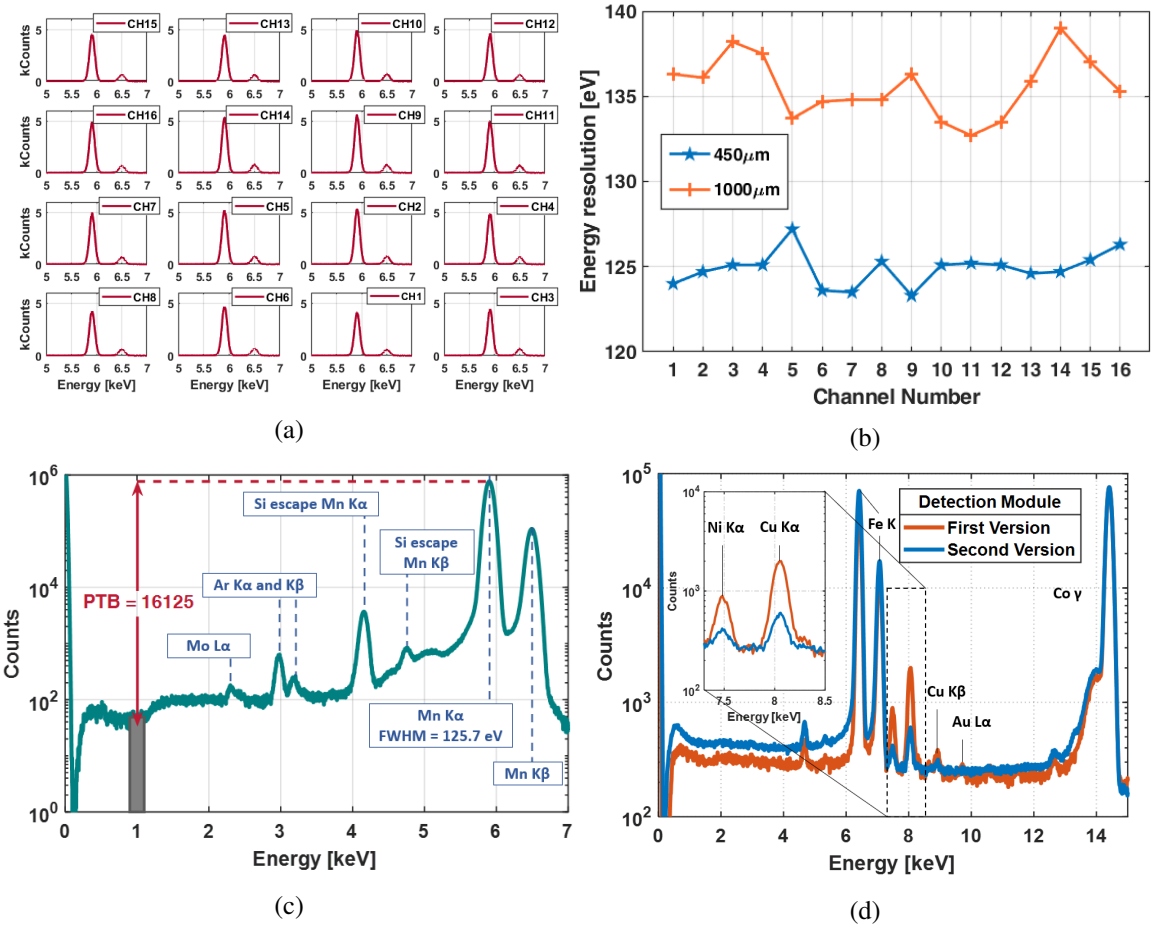

Figure 5: Detection module characterization. (a) 16 spectra acquired with an ^{55}Fe source with a 450 μm thick SDD array at low count rate, peaking time of the filter was set to 3 μs; (b) energy resolution comparison of each channel between one 450 μm thick and one 1000 μm thick array, evaluated with low count rate measurements at 3 μs peaking time; (c) sum spectrum of 16 channels used to evaluate the PTB; (d) sum spectrum taken with a ^{57}Co source to compare Cu, Ni and Au contamination in the two detection module releases.

divided by the average amplitude of the continuum in the energy range from 900 to 1100 eV (i.e., the background) [22]. To measure the PTB, the SDD element must be collimated such that the background of the SDD spectrum is only given by partial charge collection occurring near device entrance window inside the so-called dead layer; in such a way charge-sharing effects at the edge between adjacent channels are avoided. In the following measurements, no further collimation has been employed but the above-mentioned 4.5 mm side molybdenum mask. Summing up 16 ^{55}Fe spectra carried out simultaneously from each SDD element, we obtain the spectrum in figure 5c. The PTB of the sum spectrum is equal to 16125 and every element shows a PTB higher than 15000. The latter spectrum shows other peaks that are highlighted: Ar Kα and Ar Kβ (2.957 keV and 3.19 keV) present in the air, the escape peaks of Mn kα and Mn Kβ (4.159 keV and 4.75 keV) and a tiny peak of Mo Lα (2.293 keV) due to the Mo mask.

To find possible further contaminations of the spectrum at higher energies with respect to Mn K-lines, a ^{57}Co radioactive source is used, whose decay process produces Fe K fluorescence X-rays and γ photons at 14.41 keV. The resulting spectrum, obtained summing all the 16 channels, shows that there are Cu, Ni and few Au contaminations because of the module PCB. The Co γ photon has a non-negligible probability to pass through the detector and enough energy to excite chemical elements beyond, belonging to the PCB, whose fluorescence is in turn absorbed and detected by the SDDs.

Aiming at reducing the amount of contaminants, an improved PCB layout has been investigated. To decrease the contamination, we decreased the exposed copper on the PCB layer closer to the SDD array. The ^{57}Co spectra of the two detection module versions are reported in figure 5d. To compare them, spectra are normalized at the Co γ peak (14.41 keV). The Cu and Ni contaminations is now reduced by a factor of 10 and, in the spectrum carried out with the new detection module, the Au fluorescence line is not appreciable anymore. Such a change caused no worsening in detection performances.

3 ARDESIA-16 Spectrometer

ARDESIA-16 is a stand-alone and plug & play spectrometer able to host the 16-channel detection module described in the previous section. In figure 6, the architecture of ARDESIA-16 is depicted. The spectrometer mechanics turned out in a finger-like structure with relatively small sizes: the finger is 255 mm long with a 57 mm diameter and the base measures 140 mm × 170 mm × 100 mm. We designed the spectrometer allowing possible finger extension of 50 mm multiples, up to 505 mm. The tip of the finger, where the detection module lays, is designed to take up a minimal amount of space in the proximity of the sample holder. Thanks to this, the minimum sample distance in a 45° configuration (i.e., the sample placed at 45° with respect to the detector) is lowered to 20 mm. In this configuration, the solid angle covered by the detector reaches a maximum value of 0.4

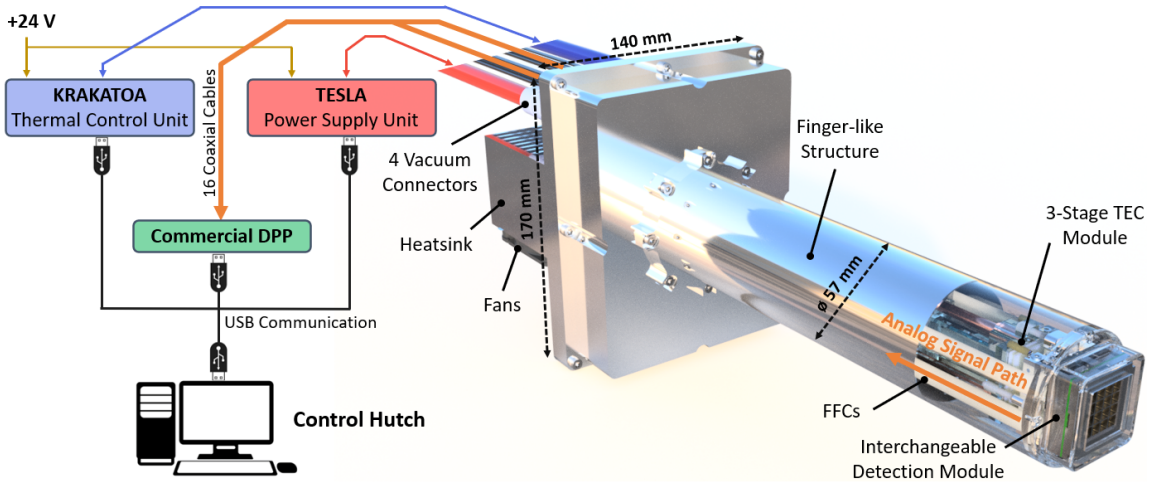

Figure 6: Render of the ARDESIA-16 spectrometer and the architecture of the complete system expected to be used in a synchrotron beamline.

sr. Nevertheless, the spectrometer allows an easy interchange of the detection module and custom adaptation to geometrical constraints of the beamlines.

The structure is compatible with high vacuum (HV) environments (i.e., $10^{-6} mbar$). The vacuum inside the instrument is guaranteed by a window, in front of the detection module, offering high X-ray transmission coefficient at low energies (i.e., < 5 keV). In the project development, we employed windows made of black Kapton, beryllium or AP5 polymer material (Moxtek, Utah, USA). The choice of the material depends on the application and the energy range of interest. Typically, beryllium is suitable for energy range down to 2 keV (P-K lines) and polymer materials allows to collect lower energy photons like C (277 eV). In spite of the lower transmission at low energy, for the first spectrometer qualification we used the cheapest and less fragile solution: black Kapton. The latter provides a transmission coefficient of about 0.5 for energy equal to 3 keV (Ar-K lines). Finally, the spectrometer can be used also window-less, sharing the same vacuum of the sample chamber.

From the base, four vacuum connectors allow the connection to the external units: Krakatoa cooling control system [2], Tesla biasing system and DPPs through 16 coaxial cables. The leakage current of the detector is lowered to a negligible value by means of a 3-stage TEC module. The detector temperature is selectable by the user and kept stable with a closed-loop regulation: an STM32 microcontroller (STMicroelectronics, Geneva, Switzerland) implements a Proportional Integral (PI) controller which acts on the current flowing in the TEC module as a function of the measured detector temperature. Three PCBs comprise the internal electronics which lays inside the instrument frame. The internal electronics performs the same tasks of the Bias PCB (section 2.2) in the characterization setup with different geometry and layout. A user-friendly MATLAB-based Graphic User Interface allows to communicate and control the spectrometer with USB connection to Krakatoa and Tesla from the control hutch. Connection to these units is necessary only for the start-up and monitoring of the system, but they can be disconnected during operation of the detector.

4 Synchrotron Qualification

The first synchrotron measurements with ARDESIA-16 were carried out at P06 beamline at PETRA III (DESY, Hamburg). The beamline features two experimental hutches: the microprobe hutch, allowing hundreds nm spot size, and the nanoprobe hutch, in which a 80 nm spot size is achievable [27, 28]. Figure 7 (a) shows ARDESIA-16 installed in the microprobe hutch. The spectrometer was mounted on a 3-axis stage and connected to the external units. The typical measurement configuration is depicted in figure 7 (b), where the sample is placed on a 3-axis motorized stage and ARDESIA-16 is placed close to it. The impinging synchrotron beam causes X-ray fluorescence and scatter emission from the sample, which is in turn detected by the spectrometer. The window, letting fluorescence inside, was made of black Kapton; however, a beryllium window is planned to be mounted for the final installation at the beamline. We equipped the spectrometer with a 450 μm thick monolithic SDD array, whose laboratory measurements are reported in figure 5 (a and c).

We assessed the count rate performance by irradiating with synchrotron light a pure manganese sample and collecting fluorescence photons with ARDESIA-16 coupled with the 16-channel Dante DPP. The spectrometer was placed at a working distance from the sample of about 30 mm and spectra were collected sweeping the incoming beam intensity. Results are reported in figure 8. Despite the

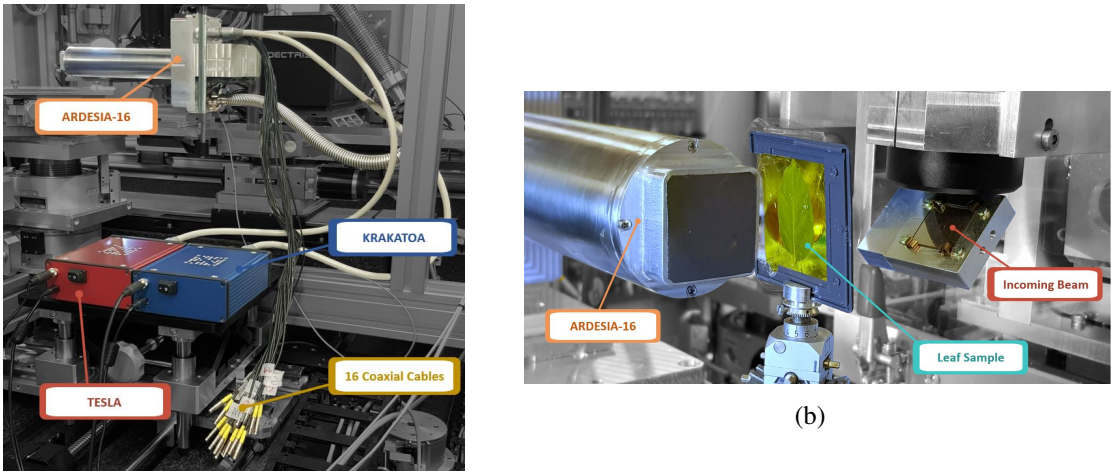

(a) (b)

Figure 7: (a) Picture of ARDESIA-16 installed at the P06 beamline (DESY, Hamburg), the external units are highlighted along with the 16 coaxial cables to be connected to the DPP. (b) Detail of the typical experimental configuration: the impinging synchrotron beam causes X-ray fluorescence and scatter emission, which is in turn collected by the spectrometer.

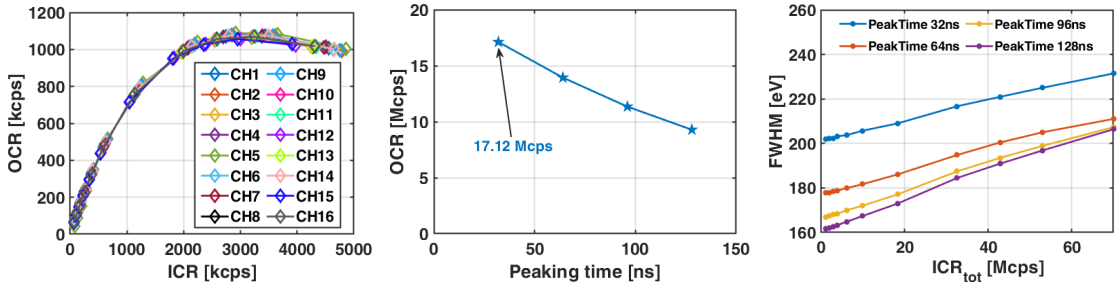

(a) (b) (c)

Figure 8: High count rate measurements. (a) OCR as a function of the ICR for each channel when the peaking time is set to 32 ns; (b) overall OCR as a function of the peaking time of the filter; (c) average energy resolution as a function of the overall ICR for different peaking time values. All measurements were carried out with flattop equal to 128 ns and the detector cooled down to −30°C.

small distance between ARDESIA and the sample, the detector showed a good homogeneity among channels (figure 8a) and a saturation of OCR to 1.1 Mcps per channel when the Input Count Rate (ICR), i.e., the measured photon rate that hits the detector, was about 3 Mcps; the peaking time was set to 32 ns (i.e., minimum achievable by DANTE) and the flattop was set to 128 ns. A trade-off exists between energy resolution and OCR; in this regard, a proper processing time must be set to fit the measurement requirements. For this purpose, sweeps of ICR have been performed at different peaking times, from 32 ns to 128 ns, whereas keeping the flattop equal to 128 ns. The overall OCR of the 16 channels as a function of the peaking time is reported in figure 8b highlighting the remarkable result of more than 17 Mcps OCR of the complete system at the minimum peaking

time. Since the processing times of each event increases with the peaking time, the OCR decreases as well; however, the achieved energy resolution improves by about 30 eV as reported in figure 8c.

We performed the first X-ray microprobing fluorescence (XFM) imaging with ARDESIA-16. For these measurements, 7 channels of the spectrometer were connected to Xspress DPPs (Quantum Detectors, United Kingdom), because those DPPs were already integrated in the P06 beamline control and data acquisition system couple with a Xspress 3 mini DPP. We placed samples on a three-axis motorized translation stage. XRF maps were acquired on an ash leaf and on a thin section of a Cr polluted soil from Altamura (Italy). The focused synchrotron light was a 300 nm × 400 nm spot-size microbeam at 15 keV energy. Figure 9a shows the Ca map (linked to the cell walls) for one measured area of the leaf with an area equal to 2 mm × 2 mm. The map was built as a function of the fitted intensity of Ca emission line after summing the 7 spectra (from 7 channels) collected for each image pixel. Each pixel is 10 μm × 10 μm and pixel counting time is 100 ms, leading to a total measurement time of about 1 hour.

Raw data from spectra, obtained with a single scan, carries information about chemical composition of the sample. As an example, we report in the figure 9b the RGB map of a region (2 mm × 3.5 mm area) of the soil sample. Each color is related to the emission of one chemical element: Fe is green, Ca is red and Cr is blue. In this case, soil analysis has been carried out to assess the possible source of Cr pollution. The co-presence of Cr and Ca in the aggregate at the centre of figure 9b, together with other evidences (Gattullo et al., 2020 [30]) allow to identify tannery sludge as the most probable Cr source. Further information about the XFM images will be published and discussed in a separated work.

5 Conclusions

In this work, we report on a state-of-the-art spectrometer for synchrotron application equipped with a 16-element monolithic SDD array. We have described the design of both the detection module and the spectrometer system reporting the performances achieved with spectroscopy measurements. Despite its compactness and the high number of SDD elements, ARDESIA-16 ranks in the high-end among X-ray spectrometers for synchrotron application in terms of energy resolution and PTB. Therefore, the use of monolithic SDD arrays is a viable solution to increase the count rate capability and the solid angle covered by the detector, without degrading the performances. Indeed, ARDESIA-16 showed an average energy resolution equal to 125 eV and a PTB higher than 15000, consistent with single element SDD performances. Finally, we carried out the first XFM images with an ARDESIA prototype, thus showing another example of application in addition to XAS and XRF, demonstrated with the previous smaller prototypes.

The ARDESIA-16 described in this work is foreseen to be installed at the P06 beamline at PETRA III (DESY, Hamburg) equipped with a Beryllium window. Moreover, a modified ARDESIA-16 is under development and will be installed at the ID16A - Nano-imaging Beamline (ESRF, Grenoble).

Acknowledgments

The project is supported by the Italian INFN — CSN5 under the ARDESIA experiment and by Politecnico di Milano. Ignazio Allegretta was supported by a research grant on the project PON

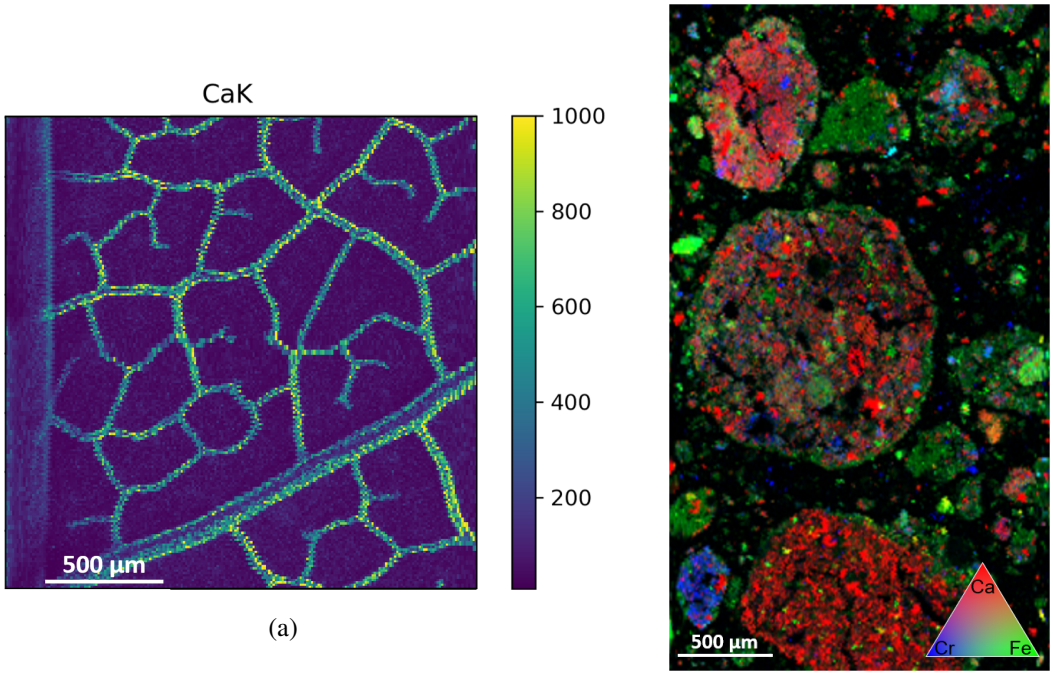

(a)

(b)

Figure 9: X-ray Fluorescence Microscopy carried out with ARDESIA-16. (a) Ca map of a region of an ash leaf; (b) RGB image of a soil sample: Red is Ca, green is Fe and blue is Cr. Images have been obtained summing spectrum data of 7 channels of the spectrometer.

R&I "Studio del sistema suolo-pianta mediante tecniche analitiche innovative che impiegano raggi X" — Progetto AIM1809249 — attività 1, linea 1. The authors would like to thank Sergio Masci for the wire bonding of the detection modules, the INFN workshop and Politecnico workshop for the production of mechanical parts.

References

[1] Hafizh, I., et al. "Characterization of ARDESIA: a 4-channel SDD X-ray spectrometer for synchrotron measurements at high count rates." *Journal of Instrumentation*, 14.06 (2019): P06027. DOI: 10.1088/1748-0221/14/06/P06027.

[2] Hafizh, I., et al. "ARDESIA: A fast silicon drift detector X-ray spectrometer for synchrotron applications." *X-Ray Spectrometry* 48.5 (2019): 382-386. DOI: 10.1002/xrs.3017

[3] G. Bellotti et al., "ARDESIA Detection Module: A Four-Channel Array of SDDs for Mcps X-Ray Spectroscopy in Synchrotron Radiation Applications." in IEEE Transactions on Nuclear Science, vol. 65, no. 7, pp. 1355-1364, July 2018, doi: 10.1109/TNS.2018.2838673.

[4] Rehr, J. J., and Albers, R. C. (2000). "Theoretical approaches to x-ray absorption fine structure." Reviews of modern physics, 72(3), 621.

[5] Gaur A, Shrivastava BD, Nigam HL. "X-ray absorption fine structure (XAFS) spectroscopy–a review." Proceedings of the Indian National Science Academy. 2013 Dec 4;79(Part B):921-66.

[6] Paunesku, T., et al. "X-ray fluorescence microprobe imaging in biology and medicine." Journal of cellular biochemistry 99.6 (2006): 1489-1502.

[7] Kopittke, P. M., et al. "Synchrotron-based X-ray fluorescence microscopy as a technique for imaging of elements in plants." Plant Physiology 178.2 (2018): 507-523.

[8] Siddons, D. P., et al. "Maia X-ray microprobe detector array system." *J. Phys.: Conf. Ser.* Vol. 499. 2014. DOI: 10.1088/1742-6596/499/1/012001.

[9] Ryan, C. G., et al. "The Maia detector and event mode." *Synchrotron Radiation News* 31.6 (2018): 21-27. DOI: 10.1080/08940886.2018.1528430.

[10] Alberti, R., et al. "Elemental mapping by means of an ultra-fast XRF spectrometer based on a novel high-performance monolithic array of Silicon Drift Detectors." *Nuclear Instruments and Methods in Physics Research Section A: Accelerators, Spectrometers, Detectors and Associated Equipment* 580.2 (2007): 1004-1007. DOI: 10.1016/j.nima.2007.06.056.

[11] Bufon, J., et al. "A new large solid angle multi-element silicon drift detector system for low energy X-ray fluorescence spectroscopy." Journal of Instrumentation 13.03 (2018): C03032.

[12] A. Rachevski, M. Ahangarianabhari, G. Aquilanti, P. Bellutti, G. Bertuccio, G. Borghi, J. Bufon, G. Cautero, S. Ciano, A. Cicuttin, et al. "The XAFS fluorescence detector system based on 64 silicon drift detectors for the SESAME synchrotron light source." Nuclear Instruments and Methods in Physics Research Section A: Accelerators, Spectrometers, Detectors and Associated Equipment, 936:719–721, 2019.

[13] Gatti, E., and Pavel R. "Semiconductor drift chamber—An application of a novel charge transport scheme." *Nuclear Instruments and Methods in Physics Research* 225.3 (1984): 608-614. 10.1016/0167-5087(84)90113-3.

[14] Gatti, E., Pavel R., and Walton J. T. "Silicon drift chambers-first results and optimum processing of signals." *Nuclear Instruments and Methods in Physics Research* 226.1 (1984): 129-141.

[15] Guruswamy, T., et al. "Beamline Spectroscopy of Integrated Circuits With Hard X-ray Transition Edge Sensors at the Advanced Photon Source." arXiv preprint arXiv:2012.11680 (2020).

[16] de Wit, M., et al. "High aspect ratio transition edge sensors for x-ray spectrometry." Journal of Applied Physics 128.22 (2020): 224501.

[17] Fano, Ugo. "Ionization yield of radiations. II. The fluctuations of the number of ions." Physical Review 72.1 (1947): 26.

[18] Bombelli, L., et al. ""CUBE", A low-noise CMOS preamplifier as alternative to JFET front-end for high-count rate spectroscopy." In *2011 IEEE Nuclear Science Symposium Conference Record.* IEEE, 2011. p. 1972-1975. DOI: 10.1109/NSSMIC.2011.6154396.

[19] Bombelli, L., et al. "High rate X-ray spectroscopy with "CUBE" preamplifier coupled with silicon drift detector." In *2012 IEEE Nuclear Science Symposium and Medical Imaging Conference Record (NSS/MIC).* IEEE, 2012. p. 418-420. DOI: 10.1109/NSSMIC.2012.6551138

[20] Quaglia, R., et al. '"Silicon drift detectors and CUBE preamplifiers for high-resolution X-ray spectroscopy." *IEEE Transactions on Nuclear Science.* 62.1 (2015): 221-227. DOI: 10.1109/TNS.2014.2379941.

[21] Lechner, P., et al. '"Silicon drift detectors for high resolution room temperature X-ray spectroscopy." *Nuclear Instruments and Methods in Physics Research Section A: Accelerators, Spectrometers, Detectors and Associated Equipment.* 377.2-3 (1996): 346-351. DOI: 10.1016/0168-9002(96)00210-0.

[22] Lechner, P., et aI., "Novel High-resolution Silicon Drift Detectors." *X-Ray Spectrom.*, vol. 33, issue 4, 256-26 1, 2004. DOI: 10.1002/xrs.717.

[23] G. Bertuccio, et al., "A silicon drift detector-CMOS front-end system for high resolution X-ray spectroscopy up to room temperature." J. Instrum. 2015, 10(1), P01022.

[24] F. Mele, M. Gandola and G. Bertuccio, "SIRIO: A High-Speed CMOS Charge-Sensitive Amplifier for High-Energy-Resolution X-γ Ray Spectroscopy With Semiconductor Detectors." in IEEE Transactions on Nuclear Science, vol. 68, no. 3, pp. 379-383, March 2021, DOI: 10.1109/TNS.2021.3055934.

[25] Hafizh, I., et al. "Assessment of analog pulse processor performance for ultra high-rate x-ray spectroscopy." Nuclear Instruments and Methods in Physics Research Section A: Accelerators, Spectrometers, Detectors and Associated Equipment 945 (2019): 162479.

[26] https://xia.com/wp-content/uploads/2018/06/FalconX8_flyer_180508.compressed.pdf

[27] Schroer, C. G., et al. "Hard X-ray nanoprobe at beamline P06 at PETRA III." *Nuclear Instruments and Methods in Physics Research Section A: Accelerators, Spectrometers, Detectors and Associated Equipment.* 616.2-3 (2010): 93-97. DOI: 10.1016/j.nima.2009.10.094.

[28] Boesenberg, Ulrike, et al. "Fast X-ray microfluorescence imaging with submicrometer-resolution integrating a Maia detector at beamline P06 at PETRA III." Journal of synchrotron radiation 23.6 (2016): 1550-1560. DOI: 10.1107/S1600577516015289.

[29] P.A. Scoullar, C.C. McLean, R.J. Evans, "Real time pulse pile-up recovery in a high throughput digital pulse processor." AIP Conf. Proc. 1412 (1) (2011) 270–277.

[30] Gattullo, C. E., et al. "Assessing chromium pollution and natural stabilization processes in agricultural soils by bulk and micro X-ray analyses." Environmental Science and Pollution Research 27.18 (2020): 22967-22979.